Single vesicle analysis of aqueous humor in pediatric ocular diseases reveals eye specific CD63-dominant subpopulations

Chen-Ching Peng[1,2], **Deborah Im**[1,2], **Shreya Sirivolu**[1,2], **Bibiana Reiser**[1,2,3], **Aaron Nagiel**[1,2,3], **Paolo Neviani**[4], **Liya Xu**[1,2], **Jesse L. Berry**[1,2,3,5]

[1]The Vision Center at Children's Hospital Los Angeles, Los Angeles, California, USA

[2]USC Roski Eye Institute, Keck School of Medicine of the University of Southern California, Los Angeles, California, USA

[3]The Saban Research Institute, Children's Hospital Los Angeles, Los Angeles, California, USA

[4]The Extracellular Vesicle Core at Children's Hospital Los Angeles, Los Angeles, California, USA

[5]Norris Comprehensive Cancer Center, Keck School of Medicine, University of Southern California, Los Angeles, California, USA

Abstract

Aqueous humor (AH), the clear fluid in front of the eye, maintains the pressure and vitality of ocular tissues. This fluid is accessible via the clear cornea which enables use of AH as a liquid biopsy source of biomarkers for intraocular disease. Extracellular vesicles are detectable in the AH and small extracellular vesicles (sEVs) are present in the AH from adults. However, EVs in AH from pediatric eyes in vivo have never previously been explored. We know very little about the heterogeneity of AH EV populations in ocular disease. Twenty-seven processing-free AH samples from 19 patients across four different pediatric ocular diseases were subjected to Nanoparticle Tracking Analysis (NTA) and Single Particle-Interferometric Reflectance Imaging Sensor (SP-IRIS) analysis. NTA demonstrated the concentration of AH EV/EPs is 3.11×10^9–1.38×10^{10} particles/ml; the majority sized 76.8–103 nm. SP-IRIS revealed distinct patterns of tetraspanin expression of AH sEVs. An enriched mono-CD63+ sEV subpopulation identified in AH indicates this is a potential AH-specific biomarker. In the setting of retinoblastoma there

was a more heterogeneous population of sEVs which normalized with treatment. This suggests a potential clinical application of direct measurement of sEV subpopulations in AH samples to monitor successful tumor response to therapy.

Keywords

aqueous humor; extracellular vesicles; ocular liquid biopsy; pediatric ocular disease; single vesicle analysis

1 | INTRODUCTION

Accurate assessment and monitoring of eye disease in children have always been challenging and often relies on clinical features alone. Mechanisms for objective molecular diagnosis combining genomic, proteomic and metabolomic translational medicine is needed and will potentially enable precise management of these diseases. Recent advances in genomics play a key role in the diagnosis and management of pediatric eye disease, and organ-specific genetic testing is becoming more common in the routine care of eye disease (Gerrish et al., 2019). Thus, innovative methods of objectively diagnosing and evaluating *organ*-specific pediatric ocular diseases is an area of great clinical need.

Evaluation of biomarkers in the aqueous humor (AH) is of particular value. The AH is a dynamic, clear fluid in the anterior chamber of the eye secreted by the ciliary body as a source of nutrition for ocular tissues and to maintain the intra-ocular pressure. As it is an eye-specific fluid, AH liquid biopsies enable diagnosis and monitoring of ocular diseases. Repeated sampling provides the ability for longitudinal data to better understand molecular dynamics associated with disease states. Even in the setting of intraocular cancer, a systematic review of AH paracentesis in retinoblastoma (Rb) demonstrated no seeding from needle tracts or evidence of metastases (Smith & Smith, 2013), illustrating the safety of AH liquid biopsy via paracentesis. Biomarkers (Berry, Xu et al., 2017; Berry et al., 2018; Gerrish et al., 2019; Xu et al., 2020) found in the cell free DNA of AH may serve as objective measures to aid in clinical management of Rb. This biomarker assessment is not unique to Rb; differential miRNA profiles (Edward et al., 2016) and inflammatory protein markers (Wu et al., 2018; Zhao et al., 2020) in AH of patients with congenital glaucoma and congenital cataracts have also been recently investigated. However, while extracellular vesicles have been hypothesized to be a key player in the ocular system and are known to be present in the AH, they have not yet been investigated in pediatric eye disease (Delsin et al., 2019).

Extracellular vesicles (EVs) is the collective term for various secreted membrane-enclosed nano-sized vesicles released by virtually every cell type (Yu et al., 2014). They have critical functions in cell-to-cell communication, and understanding their role in biological processes is essential in elucidating disease progression and response to the environment (Bordanaba-Florit et al., 2021). EVs hold proteins, nucleic acids, lipids, sugars, and membrane markers of the cells that secrete them (He et al., 2016). Most studies have relied on isolation and enrichment followed by biochemical analysis of bulk EVs separated from biofluids (Bordanaba-Florit et al., 2021). EVs in the eye are scarcer than in other biofluids due to

the blood-retinal barrier, thus EVs found in the AH are mostly secreted by intraocular tissues, making EV investigation in ocular disease even more compelling (Hsu et al., 2018). Research has shown that EVs contribute to the pathophysiology in glaucoma and age-related macular degeneration (Hsu et al., 2018). The role of myocilin protein alterations in causing glaucoma has been established, with one study reporting that myocilin-associated EV enrichment in the AH suggests a physiological importance in the regulation of trabecular drainage and thus intraocular pressure (Perkumas et al., 2007). Although informative, these approaches do not capture the dynamics of EV biogenesis, distribution and other contributions to pathophysiology (Arab et al., 2021; Bordanaba-Florit et al., 2021).

Nanoparticle tracking analysis (NTA) and Single Particle-Interferometric Reflectance Imaging Sensor (SP-IRIS) facilitates quantification and phenotyping of EV and extracellular particle (EP) subpopulations on single vesicle resolution. The optical clarity of the AH enables single vesicle analysis with unprocessed biofluid to minimize artifacts and bias generated by sample processing. However, to our knowledge, no studies have investigated EVs in the AH from pediatric eyes through a single vesicle approach. Tetraspanin proteins are organized into tetraspanin-enriched microdomains in the plasma membrane and serve a diverse number of roles such as adhesion, cell-cell fusion, endocytosis and migration (Lang & Hochheimer, 2020). Quantification of EVs, identification of particle size distribution and of EV tetraspanin expression profiles may elucidate molecular pathogenesis of eye diseases and have future clinical application. The expression profiles of common tetraspanin markers, including CD63, CD81 and CD9 were defined (Klingeborn et al., 2017; Kowal et al., 2016; Zhang et al., 2016) but whether these tetraspanins are expressed on AH-derived EVs remains unclear. In this pilot study, we evaluated 27 AH samples from 24 eyes of 19 patients with four different types of pediatric eye diseases: congenital cataract (CAT), congenital glaucoma (GLC), pediatric retinal disease (PRD) and retinoblastoma (Rb). EV subpopulations in treatment naïve retinoblastoma and treatment active retinoblastoma eyes were also evaluated. AH-derived EV/EP size distribution, EV quantification and tetraspanin subpopulation profiling was analysed by NTA and SP-IRIS, respectively.

2 | MATERIALS AND METHODS

Per MISEV2018 (Minimal information for studies of extracellular vesicles 2018) guidelines (Théry et al., 2018), EVs will be identified by bona fide markers (such as CD9+ EV) or by size (small EVs) in this publication.

2.1 | Patients and sample collection

The study was conducted under the Institutional Review Board approval at Children's Hospital Los Angeles, and it conformed to the requirements of the United States Health Insurance Portability and Privacy Act and adhered to the tenets of the Declaration of Helsinki. This publication was written adhering to MISEV2018 (Minimal information for studies of extracellular vesicles 2018) guidelines (Théry et al., 2018). Analysis was done as part of an IRB approved biorepository; parental consent was obtained from all patients from whom AH samples were taken and stored. Data was kept separate from clinical data until final analysis, which was done retrospectively. Clear corneal paracentesis was

performed with extraction of up to 0.1 ml of AH as part of the procedure of routine anterior segment surgery for congenital cataract, congenital glaucoma and pediatric retinal disease, at diagnosis or during treatment for Rb, including during intravitreal injection of chemotherapy or immediately after enucleation. Treatment of all Rb patients was carried out in a non-randomized manner per CHLA protocol (Berry et al., 2013; Berry, Bechtold et al., 2017; Berry, Kogachi et al., 2017), and treating physicians were blinded to the results of AH analyses. Samples were aliquoted and stored at −80°C until analysis. (Kim et al., 2021).

2.2 | Transmission electron microscopy (TEM)

AH samples were fixed by adding 2 μl of 16% paraformaldehyde to 14 μl of sample and mixed by gently drawing up mixture into the pipet tip three times. Immediately before adding sample, the 400 mesh coper grids with a carbon support film (EMS, Hatfield PA, USA) were made hydrophilic using a Pelco EasiGlow glow discharge unit (Ted Pella, Redding CA, USA). Four micro litre of sample/fix mixture was deposited on a grid and allowed to incubate for 6 min. This was blotted off onto filter paper, and replaced with 4 μl of NanoW (Nanoprobes, Yaphank NY, USA). After 2 min, the NanoW was blotted off, and replaced with a fresh droplet of NanoW and incubated for 2 min. This was repeated a third time with a 4-min incubation. Negative stained samples were allowed to fully air dry before imaging on a Talos F200C transmission electron microscope at 200 KeV(Thermo Fisher Scientific, Waltham MA, USA). Images were collected on a Seta CMOS 4 K camera (Thermo Fisher Scientific, Waltham MA, USA).

2.3 | Nanoparticle tracking analysis (NTA)

The nanoparticle size and concentration from 10uL unprocessed AH samples were diluted in PBS and analysed using the Nanoparticle tracking analysis system NanoSight NS300 (The Malvern Panalytical, UK) equipped with a 405 nm laser and a sCMOS camera. Under the laser path, Brownian movement of the particles in suspension was recorded by the camera and the moving tracks were analysed via Stokes-Einstein equation to get the hydrodynamic radius and the vesicle count for each modal size. Results were displayed as particle count per size distribution. Particle concentration was calculated based on the input volume. Data analysis was performed by NTA software 3.4 and the data are presented as the average and standard deviation of at least five video recordings.

2.4 | Single particle-interferometric reflectance imaging sensor (SP-IRIS) and Triton-x 100 treatment assay

Single particle interferometric reflectance imaging sensing by Exoview R100 SP-IRIS analysis was performed using the ExoView Human Tetraspanin Kit (NanoView Biosciences, USA). Desired volume (tested by serial dilution, between 0.25 and 10 ul) of unprocessed AH samples were diluted in buffer A to a final volume of 40 μl. Thirty-five micro litre of each diluted sample was incubated on ExoView Tetraspanin Chip for 16 h at room temperature. The chips were then washed three times in solution A (ExoView Human Tetraspanin Kit, NanoView Biosciences, USA) and followed by incubation with Immunocapture antibodies that consist of anti-CD9 CF488, anti-CD81 CF555, and anti-CD63 CF647. The antibodies were pre-diluted 1:500 in solution A. Two hundred and fifty microlitre of the antibody solution was added onto the remaining 250 μl solution A after the

chip washing step (1:1000, final antibodies dilution for incubation). After 1 h incubation at room temperature, the chips were washed, dried and then imaged with the ExoView R100 reader using the ExoView Scaner 3.0 acquisition software. The data was then analysed using ExoView Analyzer 3.0.

A Triton-X 100 treatment assay was performed. AH samples from one PRD and one CAT patient were diluted 1:1 with a 0.2% Triton-X 100 in PBS to achieve a final Triton-X 100 concentration of 0.1%, incubated for 10 min at room temperature and then processed on the ExoView platform as described.

2.5 | Statistical analysis

Categorical variables including eye laterality, gender and age at diagnosis were compared using the Fisher's exact test. Continuous variables were summarized as the mean ± standard error of mean (S.E.M.) and average percentages ± S.E.M. All continuous variables are non-normal distributed based on the Shapiro-Wilk testing. Non-normally distributed variables were compared by the pairwise Mann–Whitney U test. All statistical tests were two-tailed, and $p < 0.05$ was considered statistically significant. P-value were represented as: *$p < 0.05$; **$p < 0.01$; ***$p < 0.001$. All statistical analyses and plots were conducted using the Prism 8 (GraphPad).

3 | RESULTS

3.1 | Participant demographics and treatment conditions

A total of 24 eyes of 19 patients were included in the study; five patients presented with bilateral disease; two Rb patient presented for secondary enucleation after treatment. No participants withdrew consent or were lost to follow-up over the study period. Demographics and treatment conditions at the time of sample collection are summarized in Table 1. Study group comparisons had no significant differences in eye laterality, gender, or age at diagnosis: Retinal pathology (Rb + PRD) versus non-retinal pathology (CAT+GLC) and treatment naïve Rb (Diagnosis + Primary enucleation) versus treatment active Rb (Secondary enucleation + chemotherapy), but the age at diagnosis was significantly lower for Rb patients: Normal (CAT + GLC + PRD) versus tumor (Rb). Treatment courses for eye salvage were nonrandomized and decided by the treating physicians without a prior knowledge of AH biomarkers. No patients had complications secondary to AH sampling, including infection, iris trauma, synechiae, hyphema or secondary cataract. No child with Rb developed extraocular disease or metastatic disease throughout the follow-up period.

3.2 | Size, quantity and concentration of AH EV/EPs

To characterize the EVs present in pediatric AH, the morphology and distribution of particles were examined under TEM. As seen in Figure 1a, a wide-field and close-up view of an individual unprocessed pediatric AH sample revealed a membrane-enclosed particle with a round morphology.

EV/EPs were obtained and quantified in all AH samples in four different pediatric eye diseases: congenital cataract (CAT), congenital glaucoma (GLC), pediatric retinal disease

(PRD) and retinoblastoma (Rb). Rb containing eyes were evaluated in two different groups, into treatment naïve retinoblastoma (Rb_Tn) and retinoblastoma treatment active retinoblastoma (Rb_Tx) containing eyes, making a total of five different pediatric eye disease states. Unprocessed AH samples were subjected to nanoparticle tracking analysis (NTA) for EV/EP quantification and comparison between different study groups (Figure 1, Supplementary Figure 1 and Table 2). The EV/EPs were detectable in all AH samples with a dominant proportion observed at the 80~100 nm size range (Figure 1b) and the AH EV/EP concentrations were determined in 3.11×10 (Delsin et al., 2019)~1.38×10 (Yu et al., 2014) particles per mL (Figure 1c). The nanoparticle modal size (76.8~103 nm, Figure 1d) and mean size (97.4~134.5 nm, Figure 1e) of the detected AH EV/EPs were <200 nm suggesting that small EV/EPs are a major constituent in AH. Study group comparisons showed that non-tumor containing eyes (CAT + GLC + PRD) had a smaller nanoparticle mean size compared to Rb containing eyes (*P* value 0.002, Table 2). More EV/EPs were significantly detected in Rb_Tn containing eyes compared to Rb_Tx containing eyes (*P* value 0.022, Table 2), suggesting the possibility of tumor-derived EV/EPs presence in Rb_Tn which were subsequently eliminated by treatment.

3.3 | Tetraspanins expression profile and quantification of AH EVs

A non-vesicular fraction (protein aggregates or other small particles) may be present in our unprocessed AH samples. To exclude the possibility of non-vesicular observations, immunocapture-based detection method for tetraspanin markers was applied to ensure the particles analysed are truly the tetraspanin-positive vesicles. Tetraspanin markers were evaluated in all AH samples obtained in all five different disease states. Single Particle-Interferometric Reflectance Imaging Sensor (SP-IRIS) was utilized for and fluorescent-based immunophenotyping of tetraspnin CD63-AF647 (red channel), CD81-AF555 (green channel) and CD9-AF488 (blue channel) in all unprocessed 27 AH samples at a single vesicle level (Figure 2a). Total fluorescent count in each spot pre-conjugated with anti-CD63, anti-CD81 and anti-CD9 antibodies were examined in each sample (Figure 2b). By comparing the fluorescent signals from CD63-AF647, CD81-AF555 and CD9-AF488 detected in each spot, higher vesicle count of CD63-AF647 positive EVs in CD63 spot could be detected in non-tumor containing eyes and Rb_Tx AH samples among all fluorescent positive EVs suggesting the CD63 positive EVs may be the dominant EV form in AH (Figure 2c). Additionally, higher CD81/CD9+ EV than CD9 positive EV counts were detected in CAT, GLC, and PRD in the CD9 spot (Figure 2c). Interestingly, higher fluorescent vesicle count could be detected in Rb_Tn samples suggesting the presence of tumor-derived small EVs (sEVs) before chemotherapy (Figure 2d).

We next profiled the tetraspanin subpopulations in AH EVs by analyzing the distribution of fluorescent tetraspanin expression in each spot (Figure 3a). The colocalization analysis showed that the spatial overlap fluorescent particle counts between different tetraspanins in each spot. Mono-CD63+ EVs were identified to be the most dominant sEV subpopulation from AH across CAT, GLC, PRD and Rb_Tx eyes (Figure 3b). However, more diverse sEV subpopulation profile was detected in Rb_Tn AH samples (Figure 3c). By converting each sEV subpopulation fluorescent particle count among total counts (percentages), the mono-CD63+ EV was highly enriched in the CD63 spot (Figure 3d,e). Significantly lower

percentage of mono-CD63+ EVs could be determined in Rb_Tn eyes compared to Rb_Tx eyes (70.3% versus 96.1%, $p = 0.001$, Figure 3f). However, accumulation of CD9/CD63, CD63/CD81 and CD9/CD63/CD81 subpopulations in Rb_Tn was observed (Figure 3f). These results suggested that the mono-CD63+ EV may be AH specific and additional tumor-related information may be carried by other sEV subpopulations which depletes the concentration of mono-CD63+ EVs in treatment naïve Rb eyes. Interestingly, we can detect greater CD9 and CD9/CD63/CD81 subpopulations but fewer CD9/CD81 subpopulations in retinal diseases suggesting the heterogeneity of sEV subpopulations may reflect the cell origin. Taken together, the colocalization analysis indicates the AH specificity of the mono-CD63+ EVs and the clearance of sEV heterogeneity by chemotherapy.

To determine if the particles captured on the Exoview R100 chip are membrane-enclosed, we pre-treated two AH samples with Triton-X 100 before loading onto the chip. Comparing to the untreated sample, all the fluorescent-positive particle counts were strongly decreased in the Triton-X 100 treated AH samples (Supplementary Figure 2) indicating that the majority of the particles we detected in SP-IRIS are vesicles with lipid bilayer membranes.

4 | DISCUSSION

Herein we demonstrate the first evaluation of AH-derived EVs—including quantification, size analysis and expression profiling—from pediatric patients with ocular disease. We evaluated 27 AH samples from 5 different disease states: congenital cataract, congenital glaucoma, pediatric retinal disease, treatment naïve and treatment active retinoblastoma in 24 eyes of 19 patients.

NTA analysis of AH revealed that AH EV/EP concentration across pediatric disease states is at the level of 10^9–10^{10} particles per ml. This finding is consistent with previous EV studies that applied unprocessed AH as input material. Dismuke et al., identified the concentration of AH EV to be at the level of 10^8–10^9 vesicles per ml from adult cataract containing eyes (Dismuke et al., 2015), however, another group reported a concentration to the level of 10^{10}–10^{11} vesicles per ml using the pooled AH from adult diabetes and adult cataract groups (Gao et al., 2021). Further, by EV/EP sizing analysis, we determined that the diameter of the AH EV/EPs overlapped the typical small EV size range: 50–120 nm, suggesting that sEVs are the major constituent of the AH EV/EPs in pediatric eye disease. We also provide evidence that larger sized EV/EPs could be identified in AH from retinoblastoma eyes suggesting that tumor-derived EV/EPs may represent a heterogeneous population distinct from sEVs in terms of size and biogenesis (Ciardiello et al., 2020). Our investigations revealed that EVs can be identified in unprocessed AH, TEM images of AH revealed membrane-enclosed particles (Figure 1a) and confirmed that the particles analysed by NTA includes EVs.

Using a single vesicle analysis approach offers valuable biological information about the subpopulations of EVs in the AH in these pediatric patients. We found that there is a low expression of both CD81+ and CD9+ EVs, but a significant enrichment of CD63+ EVs across all eyes (Figure 3f), thus demonstrating CD63+ EVs as the dominant AH-specific EV in the eye. Furthermore, CD63+ EVs enrichment consisted of almost exclusively mono-CD63+ EVs. Hoshino et al. characterized EVs from 426 human samples including different

human biofluids and demonstrated CD63 was rarely present in human derived samples, however no ocular biofluids were evaluated (Hoshino et al., 2020). CD63 was present in 10% of human plasma, serum, lymphatic, and bile duct fluid samples. Notably, our report of mono-CD63+ EV enrichment in the AH of all samples suggests that CD63+ EV is AH-specific and not enriched in other human biofluids such as plasma. The rrCD9/CD81 EV subpopulation was dominant in the plasma of 2 Rb patients (Supplementary Figure 3). Interestingly, Otsuki et al. reports CD63+ EVs from murine retinal pigment epithelial (RPE) cells participates in cell to cell communication with macrophages (Otsuki et al., 2021). RPE cell derived EV involvement with cell to cell communication with macrophages was first suggested by the same authors in 2016 and CD63+ EVs role was only recently delineated. Macrophages are closely involved in ocular inflammation and are the source of tumor necrosis factor-α, an activator of RPE cells. Thus, implicating CD63+ EVs are involved in the pathogenesis of macrophage-driven ocular inflammation. The eye, like the brain, is an unique area of immune privilege with strict immune regulation regulated by the blood-ocular barrier (Forrester & Xu, 2012). Ciliary body and iris pigment epithelial cells, which are in contact with the AH, are involved in cell-to-cell communication in maintaining the immune system of the eye (Mochizuki et al., 2013). Importantly, our report of CD63+ EV enrichment in the AH suggests that CD63+ EV may have a role in the immunoregulatory microenvironment in the eyes. The microenvironment surrounding the immune response in the ocular system is an area of active research.

One particularly interesting aspect of our investigation is that we demonstrated that eyes with retinoblastoma had a significant increase in concentration of EV/EPs, including CD63+ EVs, compared to other pediatric eyes diseases but no significant difference in modal size or mean size distribution (Table 2). In retinoblastoma eyes before treatment (treatment naïve Rb_Tn), there was a significantly more heterogeneous EV population; this heterogeneity decreased significantly after therapy (treatment active Rb_Tx) leaving primarily mono-CD63+ EVs as is seen in the AH from other pediatric eye diseases (CAT+GLC+PRD) (Figure 3f). Thus, the heterogeneity in EVs before treatment is likely tumor-derived and the post-treatment enrichment of CD63+ EVs in AH suggests a positive treatment response demonstrating that the eye is approaching a more 'normal' ocular state with a concomitant decrease in tumor-derived EVs. This further supports that CD63+ EVs may be the most abundant and AH specific EV across multiple disease states; it may also be a potential biomarker to indicate positive treatment response in children with Rb.

However, one limitation of our study is our small sample size and further studies on large patient cohorts with orthogonal methods, such as vesicle flow cytometry will be required to validate these findings. Another limitation to this investigation is the variability of diseases represented in this study and small cohort numbers within these diseases. Larger cohort sizes within each pediatric ocular disease cohorts are needed to further validate our findings within these groups. Finally, our methodology to characterize the extracellular particles present in the AH are limited to TEM, SP-IRIS and NTA analyses, and thus we present these findings as specific to the platforms utilized in this report.

In conclusion, we present a novel study that quantifies and identifies EV subpopulations in the AH in pediatric ocular diseases. This single vesicle analysis of AH EVs further

validated the presence of sEVs as the dominant EV/EP size present in the AH and confirms that EVs are readily detectable in the AH by NTA and SP-IRIS. Additionally, our findings suggest that CD63+ EVs are specific to the AH as compared to other human biosufluids. Future studies validating CD63+ EVs as an AH-specific biomarker in both pediatric and adult ocular disease are warranted as these may serve as a critical player in the immunoregulatory system in eyes. Finally, we also offer supporting evidence that heterogenous EV subpopulations are normalized after treatment in retinoblastoma eyes, thus suggesting that tumor associated EVs in the AH could be used as a biomarker to monitor successful tumor response to treatment. However, this needs to be validated in future studies with a larger cohort of Rb eyes to evaluate response to therapy. The findings of this initial study suggest that further studies utilizing single vesicle analysis of sEVs in the AH are warranted to elucidate the ocular microenvironment and molecular cargo in pediatric eyes; using this technology there is potential to identify and validate biomarkers of multiple diseases causing childhood blindness.

Supplementary Material

Refer to Web version on PubMed Central for supplementary material.

ACKNOWLEDGEMENT

REFERENCES

Arab T, Mallick ER, Huang Y, Dong L, Liao Z, Zhao Z, Gololobova O, Smith B, Haughey NJ, Pienta KJ, Slusher BS, Tarwater PM, Tosar JP, Zivkovic AM, Vreeland WN, Paulaitis ME, & Witwer KW (2021). Characterization of extracellular vesicles and synthetic nanoparticles with four orthogonal single-particle analysis platforms. Journal of Extracellular Vesicles, 10(6), e12079. 10.1002/jev2.12079 [PubMed: 33850608]

Berry JL, Bechtold M, Shah S, Zolfaghari E, Reid M, Jubran R, & Kim JW (2017). Not all seeds are created equal: Seed classification is predictive of outcomes in retinoblastoma. Ophthalmology, 124(12), 1817–1825. 10.1016/j.ophtha.2017.05.034 [PubMed: 28655537]

Berry JL, Jubran R, Kim JW, Wong K, Bababeygy SR, Almarzouki H, Lee TC, & Murphree AL (2013). Long-term outcomes of Group D eyes in bilateral retinoblastoma patients treated with chemoreduction and low-dose IMRT salvage. [published correction appears in Pediatr Blood Cancer. Jun 2014;61(6):1147. Dosage error in article text]. Pediatric Blood & Cancer, 60(4), 688–693. 10.1002/pbc.24303 [PubMed: 22997170]

Berry JL, Kogachi K, Aziz HA, Mcgovern K, Zolfaghari E, Murphree AL, Jubran R, & Kim JW (2017). Risk of metastasis and orbital recurrence in advanced retinoblastoma eyes treated with systemic chemoreduction versus primary enucleation. Pediatric Blood & Cancer, 64(4), e26270. 10.1002/pbc.26270

Berry JL, Xu L, Kooi I, Murphree AL, Prabakar RK, Reid M, Stachelek K, Le BHA, Welter L, Reiser BJ, Chévez-Barrios P, Jubran R, Lee TC, Kim JW, Kuhn P, Cobrinik D, & Hicks J (2018). Genomic cfDNA analysis of aqueous humor in retinoblastoma predicts eye salvage:

The surrogate tumor biopsy for retinoblastoma. Molecular Cancer Research, 16(11), 1701–1712. 10.1158/1541-7786.MCR-18-0369 [PubMed: 30061186]

Berry JL, Xu L, Murphree AL, Krishnan S, Stachelek K, Zolfaghari E, Mcgovern K, Lee TC, Carlsson A, Kuhn P, Kim JW, Cobrinik D, & Hicks J (2017). Potential of aqueous humor as a surrogate tumor biopsy for retinoblastoma. JAMA Ophthalmology, 135(11), 1221–1230. [PubMed: 29049475]

Bordanaba-Florit G, Royo F, Kruglik SG, & Falcón-Pérez JM (2021). Using single-vesicle technologies to unravel the heterogeneity of extracellular vesicles. Nature Protocols, 16(7), 3163–3185. 10.1038/s41596-021-00551-z [PubMed: 34135505]

Ciardiello C, Migliorino R, Leone A, & Budillon A (2020). Large extracellular vesicles: Size matters in tumor progression. Cytokine & Growth Factor Reviews, 51, 69–74. 10.1016/j.cytogfr.2019.12.007 [PubMed: 31937439]

Delsin LEA, Salomao KB, Pezuk JA, & Brassesco MS (2019). Expression profiles and prognostic value of miRNAs in retinoblastoma. Journal of Cancer Research and Clinical Oncology, 145(1), 1–10. 10.1007/s00432-018-2773-7 [PubMed: 30350021]

Dismuke WM, Challa P, Navarro I, Stamer WD, & Liu Y (2015). Human aqueous humor exosomes. Experimental Eye Research, 132, 73–77. 10.1016/j.exer.2015.01.019 [PubMed: 25619138]

Edward DP, Mahale A, Hao H, Khan A, Hameed S, Al Jadaan I, Owaidhah O, Kondkar A, Al Shamrani M, Al Shahwan S, & K Abu-Amero K (2016). Aqueous humor microRNA profiling in primary congenital glaucoma. Journal of Translational Science, 3. 10.15761/JTS.1000169

Forrester JV, & Xu H (2012). Good news-bad news: the Yin and Yang of immune privilege in the eye. Frontiers in Immunology, 3, 338. Published 2012 Nov 27. 10.3389/fimmu.2012.00338 [PubMed: 23230433]

Gao C, Fan F, Liu X, Yang J, Zhou X, Mei H, Lin X, & Luo Y (2021). Exosomal miRNA analysis of aqueous humour of diabetes and cataract patients. Current Eye Research, 46(3), 324–332. 10.1080/02713683.2020.1797107 [PubMed: 32835529]

Gerrish A, Stone E, Clokie S, Ainsworth JR, Jenkinson H, Mccalla M, Hitchcott C, Colmenero I, Allen S, Parulekar M, & Cole T (2019). Non-invasive diagnosis of retinoblastoma using cell-free DNA from aqueous humour. [published online ahead of print, 2019 Feb 11] [published correction appears in Br J Ophthalmol. 2020;104(3):415–416]. British Journal of Ophthalmology, 103(5), 721–724. 10.1136/bjophthalmol-2018-313005

He C, Zheng S, Luo Y, Wang B (2016). Exosome theranostics: Biology and translational medicine. Theranostics, 8(1), 237–255. 10.7150/thno.21945

Hoshino A, Kim HS, Bojmar L, Gyan KE, Cioffi M, Hernandez J, Zambirinis CP, Rodrigues G, Molina H, Heissel S, Mark MT, Steiner L, Benito-Martin A, Lucotti S, Di Giannatale A, Offer K, Nakajima M, Williams C, Nogués L, … Lyden D (2020). Extracellular vesicle and particle biomarkers define multiple human cancers. Cell, 182(4), 1044–1061. e18. 10.1016/j.cell.2020.07.009 [PubMed: 32795414]

Hsu MY, Chiu CC, Wang JY, Huang CT, Huang Y-F, Liou JC, Chen C, Chen HC, & Cheng CM (2018). Paper-based microfluidic platforms for understanding the role of exosomes in the pathogenesis of major blindness-threatening diseases. Nanomaterials (Basel, Switzerland), 8(5), 310. 10.3390/nano8050310

Kim ME, Xu L, Prabakar RK, Shen L, Peng C-C, Kuhn P, Gai X, Hicks J, & Berry JL (2021). Aqueous humor as a liquid biopsy for retinoblastoma: clear corneal paracentesis and genomic analysis. Journal of Visualized Experiments: JoVE, 175, Published 2021 Sep 7. 10.3791/62939

Klingeborn M, Dismuke WM, Skiba NP, Kelly U, Stamer WD, & Bowes Rickman C (2017). Directional exosome proteomes reflect polarity-specific functions in retinal pigmented epithelium monolayers. [published correction appears in Sci Rep. Nov 2018;8(1):17327]. Science Reports, 7(1), 4901. 10.1038/s41598-017-05102-9

Kowal J, Arras G, Colombo M, Jouve M, Morath JP, Primdal-Bengtson B, Dingli F, Loew D, Tkach M, & Théry C (2016). Proteomic comparison defines novel markers to characterize heterogeneous populations of extracellular vesicle subtypes. PNAS, 113(8), E968–E977. 10.1073/pnas.1521230113 [PubMed: 26858453]

Lang T, & Hochheimer N (2020). Tetraspanins. Current Biology, 30(5), R204–R206. 10.1016/j.cub.2020.01.007 [PubMed: 32155418]

Mochizuki M, Sugita S, & Kamoi K (2013). Immunological homeostasis of the eye. Progress in Retinal and Eye Research, 33, 10–27. 10.1016/j.preteyeres.2012.10.002[crossref] [PubMed: 23108335]

Otsuki Y, Ito E, Mukai A, Ueno M, Yamawaki T, Sotozono C, Kinoshita S, & Hamuro J (2021). CD63$^+$ extracellular vesicles from retinal pigment epithelial cells participate in crosstalk with macrophages in the innate inflammatory axis. Experimental Eye Research, 205, 108496. 10.1016/j.exer.2021.108496 [PubMed: 33610602]

Perkumas KM, Hoffman EA, Mckay BS, Allingham RR, & Stamer WD (2007). Myocilin-associated exosomes in human ocular samples. Experimental Eye Research, 84(1), 209–212. 10.1016/j.exer.2006.09.020 [PubMed: 17094967]

Smith SJ, & Smith BD (2013). Evaluating the risk of extraocular tumour spread following intravitreal injection therapy for retinoblastoma: A systematic review. British Journal of Ophthalmology, 97(10), 1231–1236. 10.1136/bjophthalmol-2013-303188 [PubMed: 23740960]

Théry C, Witwer KW, Aikawa E, Alcaraz MJ, Anderson JD, Andriantsitohaina R, Antoniou A, Arab T, Archer F, Atkin-Smith GK, Ayre DC, Bach J-M, Bachurski D, Baharvand H, Balaj L, Baldacchino S, Bauer NN, Baxter AA, Bebawy M, … Zuba-Surma EK (2018). Minimal information for studies of extracellular vesicles 2018 (MISEV2018): A position statement of the International Society for Extracellular Vesicles and update of the MISEV2014 guidelines. Journal of Extracellular Vesicles, 7(1), 1535750. 10.1080/20013078.2018.1535750 [PubMed: 30637094]

Wu X, Liu Z, Wang D, Lin D, Long E, Lin Z, Chen J, Cao Q, Zhu Y, Chen C, Li X, Liu Z, Lin H, Chen W, & Liu Y (2018). Preoperative profile of inflammatory factors in aqueous humor correlates with postoperative inflammatory response in patients with congenital cataract. Molecular Vision, 24, 414–424. [PubMed: 29930475]

Xu L, Polski A, Prabakar RK, Reid MW, Chevez-Barrios P, Jubran R, Kim JW, Kuhn P, Cobrinik D, Hicks J, & Berry JL (2020). Chromosome 6p amplification in aqueous humor cell-free DNA is a prognostic biomarker for retinoblastoma ocular survival. Molecular Cancer Research, 18(8), 1166–1175. 10.1158/1541-7786.MCR-19-1262 [PubMed: 32434859]

Yu B, Zhang X, & Li X (2014). Exosomes derived from mesenchymal stem cells. International Journal of Molecular Sciences, 15(3), 4142–4157. 10.3390/ijms15034142 [PubMed: 24608926]

Zhang Z, Mugisha A, Fransisca S, Liu Q, Xie P, & Hu Z (2016). Emerging role of exosomes in retinal diseases. Frontiers in Cell and Developmental Biology, 9, 643680. 10.3389/fcell.2021.643680

Zhao Y, Deng X, Chang P, Hu M, Li Z, Zhang F, Ding X, & Zhao Y (2020). Expression profiles of inflammatory cytokines in the aqueous humor of children after congenital cataract extraction. Translational Vision Science & Technology, 9(8), 3. 10.1167/tvst.9.8.3
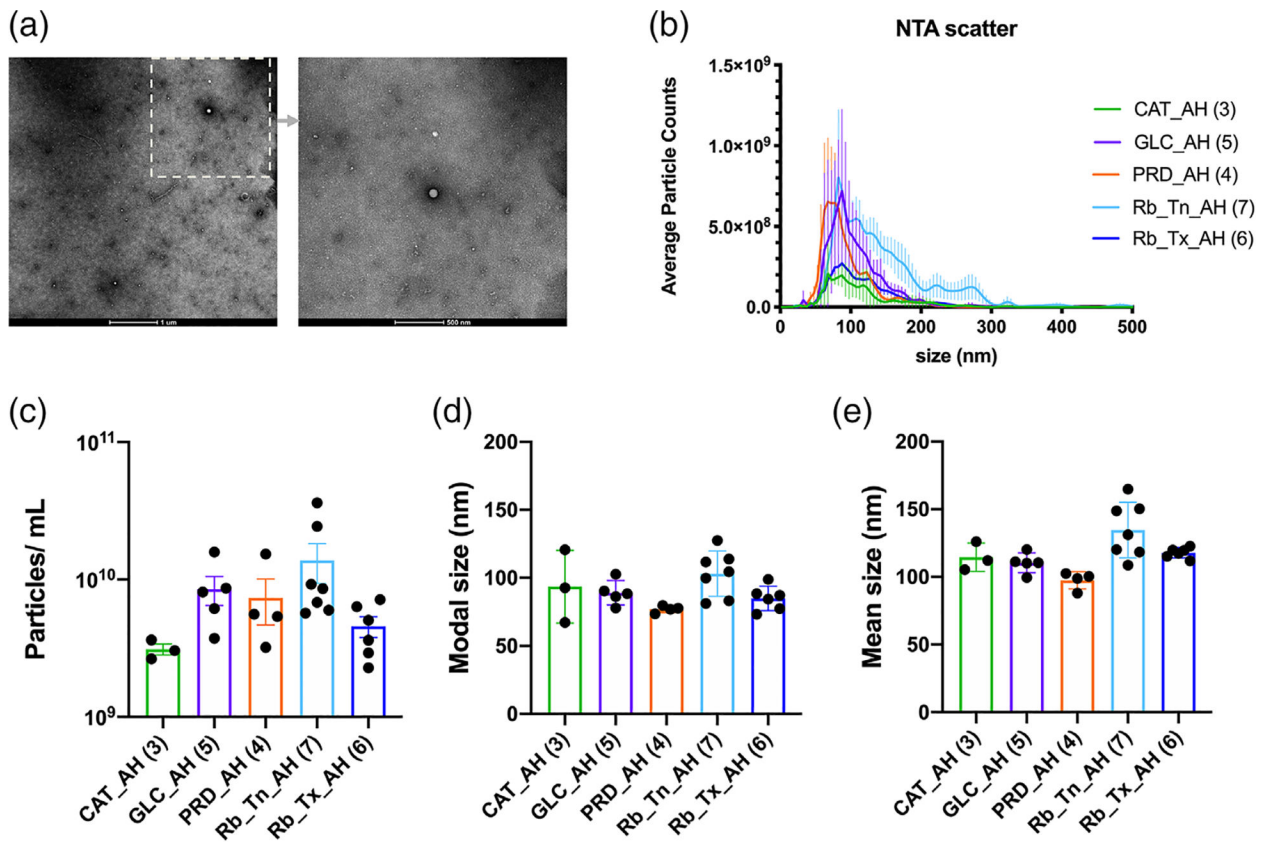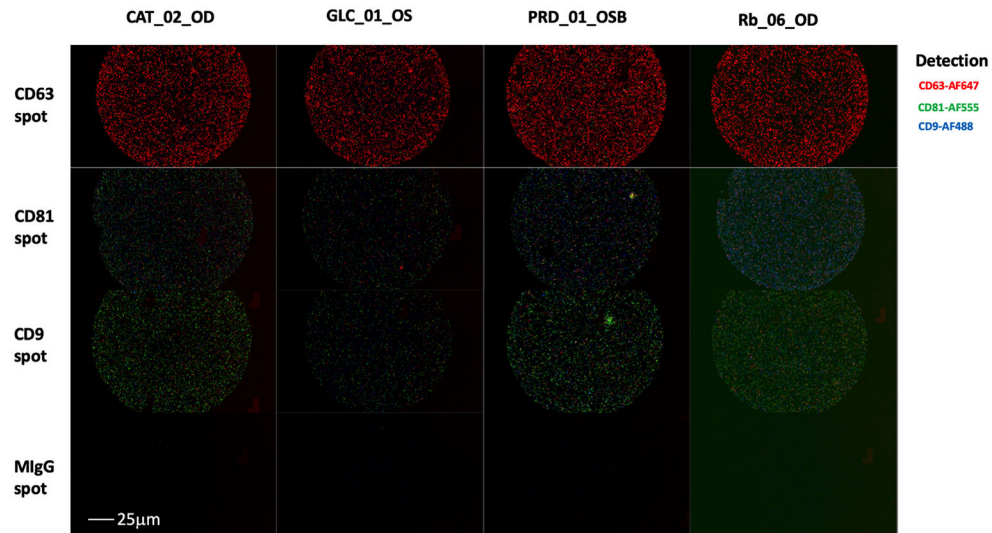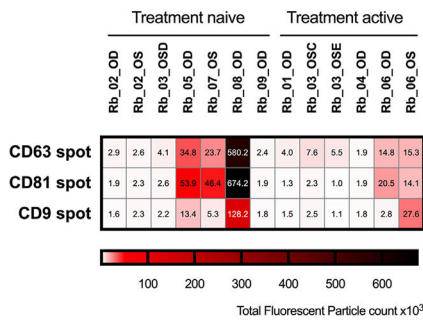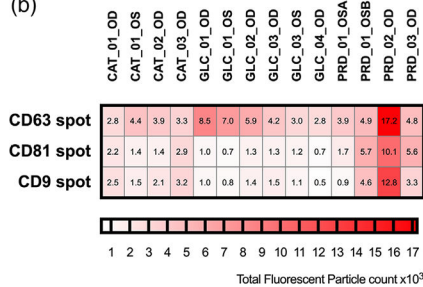
FIGURE 1.

Characterization of EV/EPs from unprocessed aqueous humor by Transmission Electron Microscopy (TEM) and NTA scatter analysis. (a) Representative TEM wide-field and close-up images of extracellular vesicles in a pediatric aqueous humor sample. (b) Average particle counts versus size distribution plots in each disease state. (c–e) Average particle concentration, modal, and mean size in each disease state. Error bars represent standard deviations obtained from each study group. See also Supplementary Figure 1 for particle counts versus size distribution plot for each sample
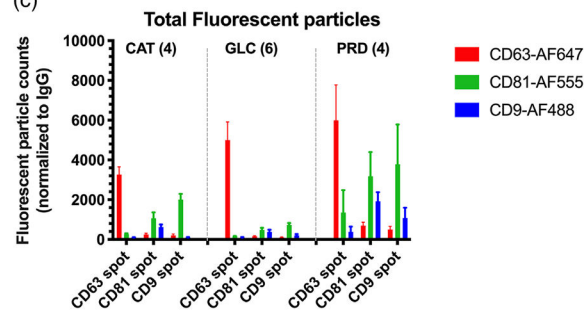
FIGURE 2.
Tetraspanin expression analysis of unprocessed aqueous humor samples using the SP-IRIS analysis. Samples were analysed by the Exoview R100 system. (a) Representative fluorescent images detected by fluorescent-conjugated antibodies (red: CD63-AF647, green: CD81-AF555 and blue: CD9-AF488) on Exoview tetraspanin chip immunocapture spots. (a) Total fluorescent particle counts normalized to isotype control IgG on a single capture spot in individual samples. (c,d) Total fluorescent particle counts normalized to isotype control IgG determined by detection antibody on three capture spots in five pediatric disease states. Error bars represent ± one S.E.M
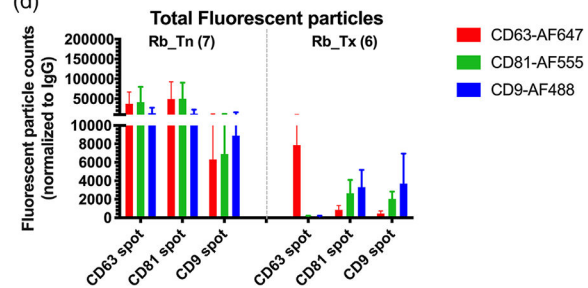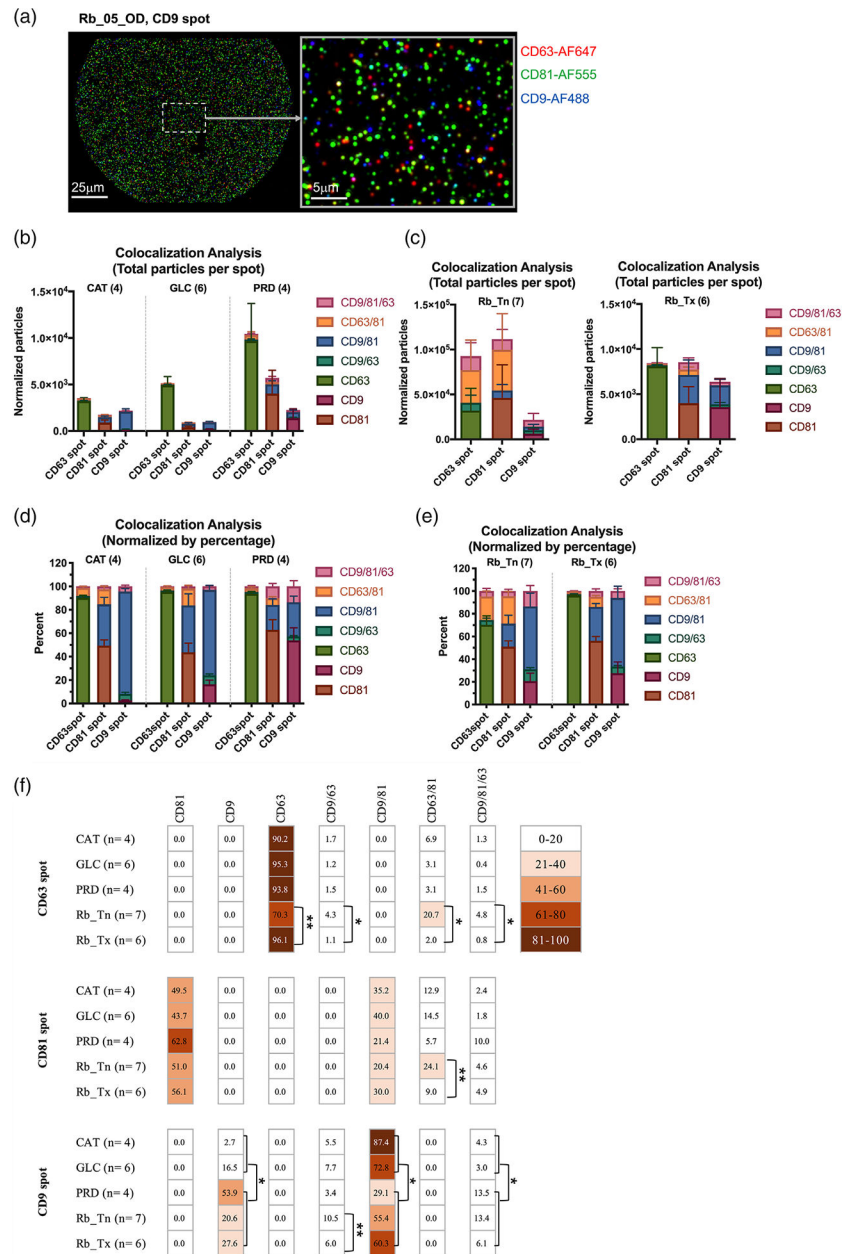
FIGURE 3.

Colocalization analysis of tetraspanin subgroups of unprocessed aqueous humor samples using the SP-IRIS analysis. Samples were analysed by the Exoview R100 system. (a) Representative fluorescent images detected by fluorescent-conjugated antibodies (red: CD63-AF647, green: CD81-AF555 and blue: CD9-AF488) on one immunocapture spot. (b,c) Tetraspanin subpopulation distribution in five pediatric disease states. Data were denoted as normalized fluorescent particle counts. (d–f) Percentages of tetraspanin subpopulation distribution in five pediatric disease states. Error bars represent ± one S.E.M. * $p < 0.05$, ** $p < 0.01$ calculated by Mann-Whitney U test

TABLE 1

Clinical demographic for each study participant eye

Patient	Eye_ID	Disease	Eye	Gender	Age at Dx (mos)	Treatment when sample collected
CAT_01	CAT_01_OD	CAT	OD	Male	168	CE/AV/IOL
CAT_01	CAT_01_OS	CAT	OS	Male	168	CE/AV/IOL
CAT_02	CAT_02_OD	CAT	OD	Male	1	CE/AV
CAT_03	CAT_03_OD	CAT	OD	Male	4	CE/AV
GLC_01	GLC_01_OD	GLC	OD	Male	4	Trabeculotomy
GLC_01	GLC_01_OS	GLC	OS	Male	4	Trabeculotomy
GLC_02	GLC_02_OD	GLC	OD	Female	50	Trabeculotomy
GLC_03	GLC_03_OD	GLC	OD	Female	168	Trabeculotomy
GLC_03	GLC_03_OS	GLC	OS	Female	168	Trabeculotomy
GLC_04	GLC_04_OD	GLC	OD	Female	196	Aqueous shunt revision right eye
PRD_01	PRD_01_OSA	PRD	OS	Male	179	Vitrectomy
PRD_01	PRD_01_OSB	PRD	OS	Male	179	Vitrectomy
PRD_02	PRD_02_OD	PRD	OD	Male	138	Vitrectomy, lensectomy
PRD_03	PRD_03_OD	PRD	OD	Male	15	pars plana vitrectomy OD
Rb_01	Rb_01_OD	Rb	OD	Female	2	Secondary enucleation
Rb_02	Rb_02_OD	Rb	OD	Female	4	Diagnosis
Rb_02	Rb_02_OS	Rb	OS	Female	4	Diagnosis
Rb_03	Rb_03_OSD	Rb	OS	Male	22	Diagnosis
Rb_03	Rb_03_OSC	Rb	OS	Male	22	Carboplatin
Rb_03	Rb_03_OSE	Rb	OS	Male	22	Secondary enucleation
Rb_04	Rb_04_OD	Rb	OD	Male	30	Intra-arterial chemotherapy for salvage
Rb_05	Rb_05_OD	Rb	OD	Male	25	Primary enuleation
Rb_06	Rb_06_OD	Rb	OD	Male	9	Carboplatin, etoposide, vincristine systemic chemotherapy for salvage
Rb_06	Rb_06_OS	Rb	OS	Male	9	Carboplatin, etoposide, vincristine systemic chemotherapy for salvage
Rb_07	Rb_07_OS	Rb	OS	Male	24	Diagnosis
Rb_08	Rb_08_OD	Rb	OD	Female	24	Primary enuleation
Rb_09	Rb_09_OD	Rb	OD	Male	2	Diagnosis

Study group comparison

P-Value	Eye (Fisher)	Gender (Fisher)	Age at Dx (MWU)
Normal (14) vs. Tumor (13)	0.704	0.999	0.045*
Retina (17) vs. Non-Retina (10)	0.448	0.415	0.464
Rb naïve (7) vs. Treatment active (6)	0.999	0.559	0.960

Abbreviations: CAT, congenital cataract; GLC, congenital glaucoma; PRD, pediatric retinal disease; Rb, retinoblastoma; OD, oculus dextrus; OS, oculus sinister; CE, cataract extraction; AV, anterior vitrectomy; IOL, intraocular lens.

Normal (CAT+GLC+PRD), Tumor (Rb); Retina (Rb+PRD), Non-retina (CAT+GLC); Rb naïve (Diagnosis+Primary enucleation), Treatment active (Secondary enucleation+chemotherapy); Fisher (Fisher's extract test), MWU (Mann-Whitney U test).

TABLE 2

Summary of nanoparticle tracking analysis

	# of samples	Concentration (Particles/ml)		Modal size (nm)		Mean size (nm)	
		Average	SEM	Average	SEM	Average	SEM
CAT	3	3.11E+09	2.85E+08	93.4	15.5	114.4	6.1
GLC	5	8.47E+09	2.02E+09	89.0	4.0	110.2	3.3
PRD	4	7.36E+09	2.70E+09	76.8	1.3	97.4	3.2
Rb_Tn	7	1.38E+10	4.45E+09	103.0	6.3	134.5	7.7
Rb_Tx	6	4.55E+09	7.90E+08	84.8	3.7	117.7	1.6
Study group comparison							
P-Value (Mann-Whitney U test)		**Conc.**		**Modal size**		**Mean size**	
Normal (12) vs. Tumor (13)		0.538		0.205		0.002**	
Retina (17) vs. Non-retina (8)		0.669		0.711		0.374	
Rb naïve (7) vs. Treatment active (6)		0.022*		0.073		0.138	

Abbreviations: CAT, congenital cataract; GLC, congenital glaucoma; PRD, pediatric retinal disease; Rb_Tn, retinoblastoma treatment naïve; Rb_Tx, retinoblastoma treatment active. Normal (CAT+GLC+PRD), Tumor (Rb); Retina (Rb+PRD), Non-retina (CAT+GLC); Rb naïve (Diagnosis+Primary enucleation), Treatment active (Secondary enucleation+chemotherapy).